DEVELOPMENT AND TESTING OF A DUAL-OBJECTIVE SYNERGISTIC CONTROL SYSTEM FOR TRANSPLANTER LATERAL LEVELING AND PLANTING DEPTH
/
移栽机横向调平与栽植仿形协同控制系统开发与测试

He CHANG [1,2], Xuedong ZHANG [1,2], Wei CUI [1,2 *], Qian ZHU [1,2], Chuandong WU [1,2], Liulei ZHOU [1,2]
[1]Chinese Academy of Agricultural Mechanization Sciences Group Co., Ltd., Beijing 100083, China
[2]State Key Laboratory of Agricultural Equipment Technology, Beijing 100083, China
Tel:+86 18339458517; E-mail: changhe0228@163.com
DOI: https://doi.org/10.35633/inmateh-77-66

Keywords: *Transplanter; Synergistic control; STSMC-ADRC; Hilly and mountainous areas*

ABSTRACT
This study develops a dual-objective control system to enhance transplanter performance on uneven terrain by synergistically integrating lateral leveling and longitudinal depth profiling. A kinematic analysis revealed strong motion coupling, which is effectively decoupled using a novel Super-Twisting Sliding Mode Active Disturbance Rejection Control (STSMC-ADRC). Co-simulation and field tests confirmed the superiority of STSMC-ADRC over conventional PID and ADRC, demonstrating faster response, minimized steady-state error, and robust disturbance rejection. The proposed strategy significantly improves platform stability and planting depth consistency, offering a robust solution for slope operations.

摘要
为解决移栽机在不平坦地形上作业出现的机体倾斜和种植深度不一致的问题，本研究开发了一种集横向平整和纵向仿形为一体的双目标协同控制系统。运动学模型确定了这些运动之间存在耦合。为有效解耦并抑制干扰，提出一种新的超螺旋滑动自抗扰控制（STSMC-ADRC）策略。通过协同仿真和现场测试表明，STSMC-ADRC 控制器的性能明显优于传统 PID 和标准 ADRC。实现更快响应、减少了稳态误差并具有卓越抗扰动能力，在动态田间条件下实现更稳定的种植深度。该系统被证明是提高移栽机在复杂斜坡上性能的稳健解决方案。

INTRODUCTION

Transplanting technology, recognized as an efficient cultivation method, presents distinct advantages over direct seeding (*Cui Zhichao et al., 2020*). It accelerates the crop growth period by approximately 15 days, thereby mitigating adverse weather conditions such as early spring low temperatures and late spring cold spells (*Ji D. et al., 2023*). Additionally, it enhances seedling survival rates, alleviates conflicts between accumulated temperature and crop succession, and ultimately increases both yield and income (*Zhou M. et al., 2024*). Consequently, transplanting has become a prevalent practice for vegetables, tobacco, and medicinal herbs—particularly in hilly and mountainous regions.

In these areas, conventional transplanters frequently experience tilting on steep or uneven slopes. This instability complicates the maintenance of consistent planting depth and diminishes transplanting quality. As manual transplanting remains predominant in these contexts, large-scale production is constrained. Therefore, there is a pressing need for equipment capable of adapting to complex terrain. This study aims to address this challenge by exploring automatic leveling and planting depth control mechanisms for transplanters with the objective of enhancing stability, safety, and uniformity in operation.

Numerous researchers have examined leveling systems for agricultural machinery. The hillside tractor developed in the United States (*Schillinger W.F. et al., 2010; McCool W.A.D.K., 2010*) and the AL QUATTRO EVO wheat harvester from Italy (*Sun Y. et al., 2020*) are designed to operate on sloped terrain; however, they are relatively large and not well-suited for small plots. Compact equipment is more appropriate for hilly areas. *Lee S,S. et al. (2000)* and *Denis D. et al. (2016)* have enhanced vehicle leveling and stability through the use of sensors, hydraulic mechanisms, and adaptive estimation techniques. These studies provide valuable insights into transplanter leveling systems.

Control strategies form the foundation of leveling systems. Proportional-Integral-Derivative (PID) control is widely used due to its simplicity (*Liu Pingyi et al., 2017*). Researchers have improved PID performance by incorporating Kalman filters (*Yang Yang et al., 2022*) as well as parameter tuning methods (*Somefun O. A. et al., 2021; Cai Zengbin, 2023*).

However, PID control has limitations when applied to nonlinear and time-varying systems; thus, fuzzy control emerges as a more suitable alternative in such scenarios (*Tang K. S. et al., 2001*). *Zhang Fugui et al, (2023), Ye Fan, (2023), Ke Chao et al, (2023),* and *Hou Pengfei, (2023)* implemented fuzzy PID controllers across various machines resulting in enhanced leveling accuracy along with faster response times. These findings underscore the potential benefits associated with intelligent control strategies.

Planting depth is another key factor for transplanting quality. Consistent depth ensures uniform soil conditions for seedlings, thereby shortening recovery time and improving survival (*Cui Zhichao et al., 2020; Zhang Qingsong et al., 2018*). Uneven terrain makes depth control difficult, and manual adjustment is inefficient (*Saeys W. et al., 2007*). Existing methods include passive profile-following, active hydraulic systems, and manual adjustment (*Han Zhenhao et al., 2018; Chen Baocheng et al., 2015; Wu Wei et al., 2013; He Zhitao et al., 2014*). Each has limitations in adaptability or complexity. Automatic depth control is therefore essential (*Xiao Mingtao et al., 2019*).

Although few studies focus directly on transplanters, related research provides references. *Saeys W. et al, (2007),* achieved precise fertilizer depth control. *Cai Guohua et al, (2011),* developed furrowing depth control, and *Han Bao et al., (2018),* applied PID for soil-engaging depth. *Yang Yinhui et al., (2007),* monitored header height with ultrasonic sensors. *Li Mingsheng et al., (2013)*, and *Ma Yong et al., (2019),* used fuzzy PID with force and position feedback for tillage depth control. These studies demonstrate fast response and good adaptability, providing foundations for transplanter depth control.

In summary, existing studies mainly emphasize longitudinal profiling, while lateral leveling and the influence of external disturbances remain underexplored. To fill this gap, this paper proposes a synergistic control system that combines lateral leveling and longitudinal profiling for transplanters. By monitoring terrain, platform inclination, and planting height in real time, the system achieves accurate leveling and consistent planting depth. This improves stability, adaptability, and overall performance of transplanters in slope operations.

MATERIALS AND METHODS

System Description and Kinematic Modeling

Mechanical Structural Description of the Transplanting Platform

The proposed dual-objective synergistic control system for the transplanter, which integrates lateral leveling and planting depth regulation, consists of three main components: a sensing unit, a controller, and a servo drive unit, as shown in Fig.1.

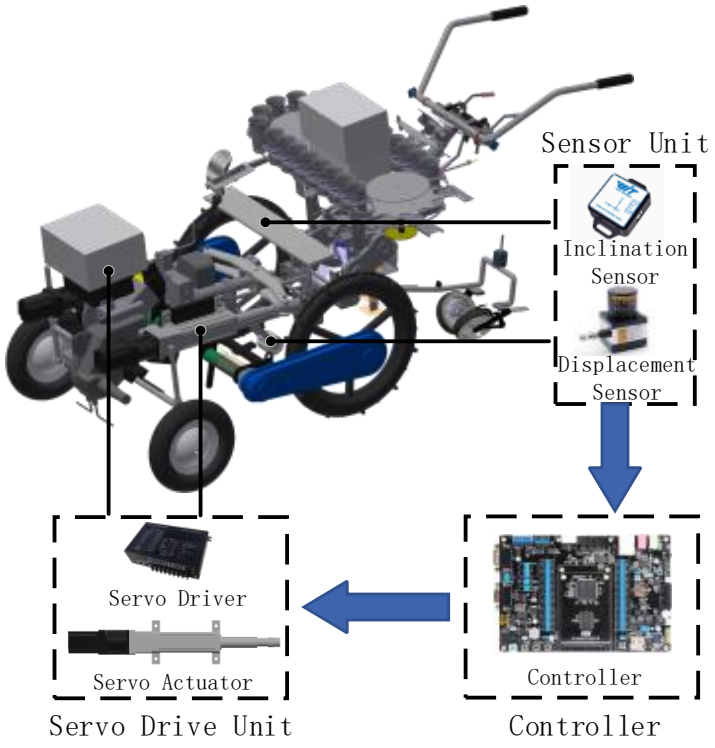

Fig. 1 – Overall Architecture of the Collaborative Control System

The sensing unit includes a tilt sensor (Witmotion WT91) and a displacement sensor (BRT38-0.5M-R2M4096-RT0.5-IP68). The tilt sensor is employed to detect changes in the lateral inclination angle of the vehicle body. It is mounted on the seedling claw mounting plate, which maintains a parallel state with the vehicle body at all times. The draw-wire displacement sensor is used to measure the distance variation between the ridge surface and the planting mechanism. The displacement sensor is fixed onto its mounting bracket.

As shown in Fig. 2, its cable end is connected to the wheel center of the profiling wheel, which maintains real-time contact with the ridge surface. When the profiling mechanism floats, the cable of the draw-wire displacement sensor extends or retracts accordingly, enabling real-time detection of the distance between the planting mechanism and the ridge surface.

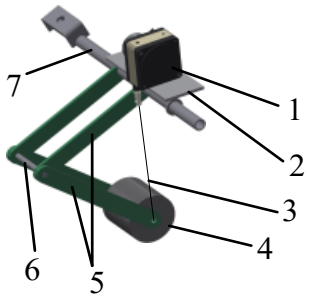

Fig. 2 - Schematic Diagram of Profile-Following Mechanism and Displacement Sensor Installation

1. Displacement sensor; 2. Displacement sensor mounting plate; 3. Displacement sensor pull cord; 4. Profile-following wheel; 5. Profile-following arm; 6. Connecting shaft; 7. Fixed bracket

The controller (STM32F103ZET6), via signal amplification and filtering circuits, acquires data from the tilt sensor through digital communication. The servo drive unit consists of a servo drive (IDS850PRO) and a servo electric cylinder (QDA75-L100). The servo drive is responsible for receiving the voltage control signal output by the controller, thereby enabling the actuation of the servo electric cylinder.

To facilitate the description and analysis of the lateral leveling and planting profiling movements of the transplanter, the machine's structure is simplified. Fig. 3 shows the schematic diagram of the mechanical structure for the transplanter's lateral leveling and planting profiling. The front axle attitude adjustment mechanism operates as a passive adjustment, capable of adapting according to terrain variations. A swing mechanism is symmetrically installed on both the left and right sides of the rear axle. This swing mechanism primarily serves the dual functions of achieving lateral leveling and planting profiling for the transplanter.

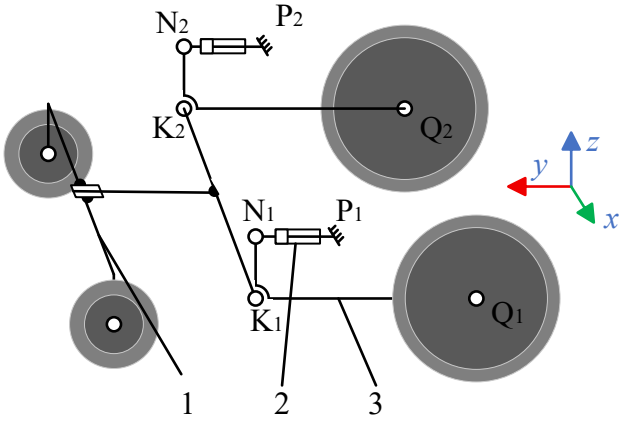

Fig. 3 - Simplified Diagram of Transplanter Structure

1. Front Axle Attitude Adjustment Mechanism; 2. Servo Electric Cylinder; 3. Oscillation Mechanism

The simplified swing mechanism is depicted in Fig. 4, where the dashed lines represent the initial state of the mechanism when the transplanter is not leveled. When the transplanter is tilted to the left and requires adjustment to a horizontal state, the servo electric cylinder of the left swing mechanism retracts, as shown in Fig. 4(a), causing the swing mechanism to rotate clockwise around the rear axle shaft. Simultaneously, the servo electric cylinder of the right swing mechanism extends, as shown in Fig. 4(b), inducing a counter-clockwise rotation around the rear axle shaft. These coordinated actions continue until the lateral inclination of the transplanter reaches the desired horizontal state.

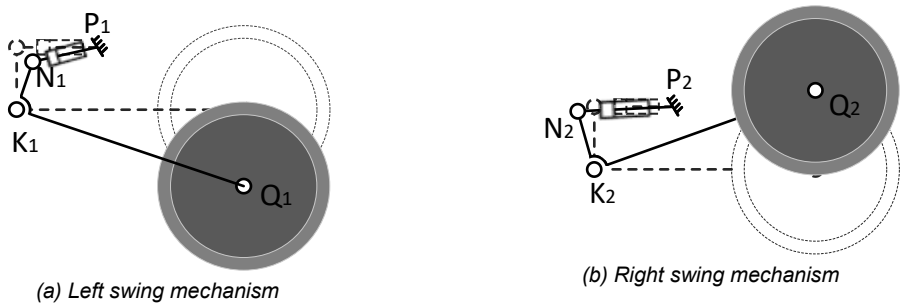

(a) Left swing mechanism (b) Right swing mechanism

Fig. 4 - Leveling mechanism schematic of the transplanting machine

When the transplanter only needs to perform profiling, as shown in Fig. 5, the dashed lines indicate the initial state of the swing mechanism before profiling is engaged. When the ridge surface exhibits a convex profile, the servo electric cylinders of both the left and right swing mechanisms retract, as illustrated in Fig. 5(a). This causes both swing mechanisms to rotate clockwise simultaneously, thereby raising the planting mechanism to the desired height. Conversely, when the ridge surface exhibits a concave profile, the servo electric cylinders of both swing mechanisms extend, as shown in Fig. 5(b). This results in both swing mechanisms rotating counterclockwise simultaneously, lowering the planting mechanism to the desired height.

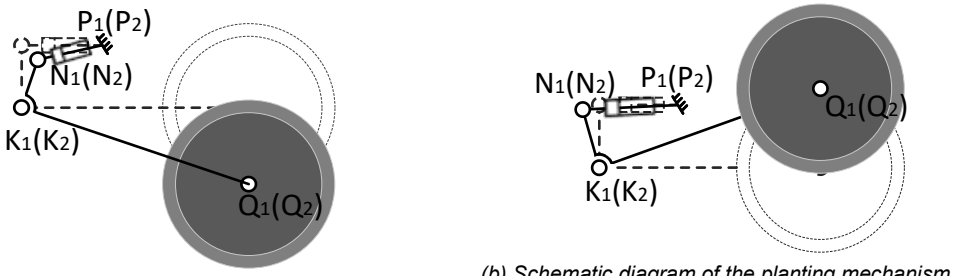

(a) Schematic diagram of the planting mechanism raising action (b) Schematic diagram of the planting mechanism lowering action

Fig. 5 - Schematic diagram of the transplanting machine's contouring

Kinematic Modeling

Kinematics is a branch of classical mechanics that primarily investigates the geometric properties of object motion, without considering dynamic factors such as the forces or masses causing the motion. Its core focus is describing the change in an object's state of motion in space over time. The leveling motion and the profiling motion are simplified as the motion of rigid bodies. The leveling motion is analyzed in the XOZ plane, while the profiling motion is analyzed in the YOZ plane. The target lateral inclination angle of the platform is defined as φ, and the target height of the platform is defined as H.

(1) Leveling Motion

The changes in H_1 and H_2 determine the rotational swing of the planting platform in the lateral horizontal direction. Here, H_1 represents the distance between the right rear wheel center and the planting platform, H_2 represents the distance between the left rear wheel center and the planting platform, R is the rear wheel radius, ΔH is the relative change between the rear wheel center and the planting platform during the process of adjusting the transplanter platform from its initial position to a horizontal state, φ is the adjustment angle for achieving lateral leveling, and the width of the transplanter platform is consistent with the length of the rear axle shaft, denoted as W.

Based on the simplified model in Fig. 6, the relationship between ΔH, φ, and W can be derived as:

$$\Delta H_t = \frac{W \tan \varphi_d}{2} \quad (1)$$

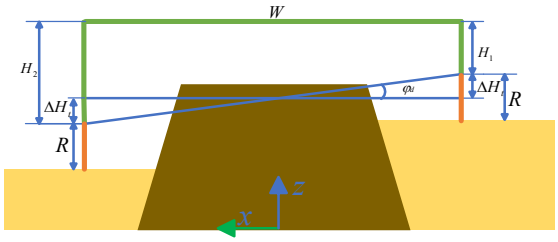

Fig. 6 - Schematic Diagram of Lateral Leveling Kinematics

(2) Profiling Motion

The movement of the transplanter's profiling mechanism causes the extension and retraction of the displacement sensor, enabling the detection of the distance between the planting platform and the ridge surface, as shown in Fig. 7. ΔH_f represents the displacement variation between the planting platform and the ridge surface detected by the displacement sensor, and H_a denotes the desired height under the initial state.

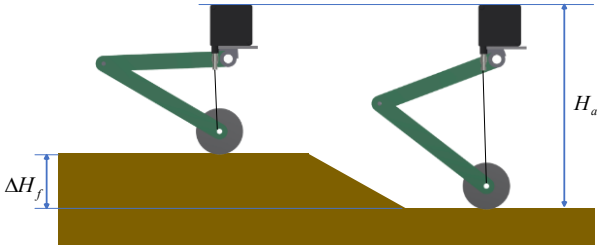

Fig. 7 - Schematic Diagram of the Kinematic Model for Elevation Contour Adjustment of the Planting Mechanism

(3) Kinematic Model of Synergistic Motion

Based on the description of the transplanter's leveling motion and profiling motion, when the transplanter performs leveling and profiling actions simultaneously, the displacement variation ΔH_l between the left wheel center and the planting platform, and the displacement variation ΔH_r between the right wheel center and the planting platform are given by:

$$\begin{cases} \Delta H_l = \Delta H_t + \Delta H_f \\ \Delta H_r = \Delta H_t - \Delta H_f \end{cases} \quad (2)$$

As shown in Fig. 8, in the initial state, $N_1'K_1$ of the left and right swing mechanisms is perpendicular to the push rod $N_1'P_1$. L_1' and L_2' are the initial lengths of the left and right servo electric cylinders, respectively, and are equal. L_d is the length of the short arm of the swing mechanism, and L_c is the length of the long arm. L_1 and L_2 are the lengths of the servo electric cylinders after changes. The swing angle of the left swing mechanism after combining the leveling motion and profiling motion is β_l , and the swing angle of the right swing mechanism is β_r . Based on the geometric relationships, the following can be derived:

$$\begin{cases} \sin\beta_l = \dfrac{\Delta H_l}{L_c} \\ \sin\beta_r = \dfrac{\Delta H_r}{L_c} \end{cases} \quad (3)$$

$$\begin{cases} \Delta L_1 = L_1' - L_1 \\ \Delta L_2 = L_2 - L_2' \end{cases} \quad (4)$$

$$\begin{cases} L_1 = (L_d - L_d \bullet \cos\beta_l)^2 + (L_1' - L_d \bullet \sin\beta_l)^2 \\ L_2 = (L_d - L_d \bullet \cos\beta_r)^2 + (L_2' + L_d \bullet \sin\beta_r)^2 \end{cases} \quad (5)$$

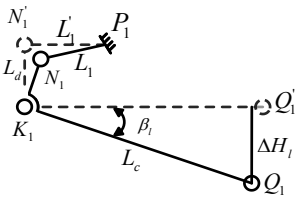

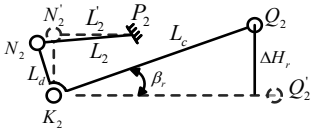

(a) Kinematic diagram of left swing mechanism *(b) Kinematic diagram of right swing mechanism*

Fig. 8 - Kinematic diagram of coordinated control swing mechanism

Combining equations (1) to (5) yields the inverse kinematic equations (6) and (7)

$$\Delta L_1 = L_1^{'} - (L_d - L_d \bullet \cos(\arcsin(\frac{\frac{W \bullet \tan\varphi}{2} + \Delta H_f}{L_c})))^2 - (L_1^{'} - L_d \bullet (\frac{\frac{W \bullet \tan\varphi}{2} + \Delta H_f}{L_c}))^2 \quad (6)$$

$$\Delta L_2 = (L_d - L_d \bullet \cos(\arcsin(\frac{\frac{W \bullet \tan\varphi}{2} - \Delta H_f}{L_c})))^2 + (L_2^{'} + L_d \bullet (\frac{\frac{W \bullet \tan\varphi}{2} - \Delta H_f}{L_c}))^2 - L_2^{'} \quad (7)$$

Equations (6) and (7) reveal that a coupling phenomenon occurs during the synergistic control of the transplanter's lateral leveling and profiling, indicating that the leveling and profiling motions influence each other.

Servo Electric Cylinder Design

The servo electric cylinder serves as the driving force source for the leveling and profiling actions of the transplanter. To accurately characterize its dynamic and kinematic properties, a mathematical model of the servo electric cylinder is established. This model describes and analyzes the system's dynamic performance indicators, enabling precise control over the extension/retraction displacement and velocity of the servo electric cylinder. The development of this mathematical model encompasses the formulation of models for both the servo motor and the transmission system.

A low-voltage DC servo motor is employed as the actuator for the transplanter. In the following expressions: L represents the armature inductance, i is the armature current, R is the armature resistance, K_e denotes the back EMF constant, ω is the motor rotational speed, J is the moment of inertia of the motor rotor, T is the motor torque, B is the friction coefficient, T_L is the load torque, K_t is the torque constant of the servo motor, and θ_m is the angular displacement of the motor. The mathematical model of the servo motor is given by:

$$\begin{cases} U = L\dfrac{di}{dt} + Ri + K_e\omega \\ J\dfrac{d\omega}{dt} = T - B\omega - T_L \\ T = K_t i \\ \omega = \dfrac{d\theta_m}{dt} \end{cases} \quad (8)$$

The input to the motor drive system is U, and the external disturbance variable is the load torque T. The angular displacement of the motor, θ_m, is taken as the output. Performing the Laplace transform on equation (8) yields equation (9):

$$\begin{cases} U(s) = Lsi(s) + Ri(s) + K_e\omega(s) \\ Js\omega(s) = T(s) - B\omega(s) - T_L(s) \\ T(s) = K_t i(s) \\ s\theta_m(s) = \omega(s) \end{cases} \quad (9)$$

Taking the angular displacement of the servo motor as the input to the transmission system, the angular displacement input to the lead screw shaft after passing through the speed reducer is θ_{BS}. The angular displacement of the lead screw shaft is then converted into the linear displacement L_x of the electric cylinder push rod via the linear bearing. The mathematical model of the transmission system is given by:

$$\begin{cases} \theta_m = \dfrac{\theta_{BS}}{n} \\ L_x = \dfrac{p_h\theta_{BS}}{2\pi} \end{cases} \quad (10)$$

where n is the speed reducer ratio, and p_h is the lead screw pitch.

Performing the Laplace transform on equation (10):

$$\begin{cases} \theta_{BS}(s) = \dfrac{\theta_m(s)}{n} \\ L_x(s) = \dfrac{p_h\theta_{BS}(s)}{2\pi} \end{cases} \quad (11)$$

Combining equation (9) and equation (10), and neglecting external disturbances, the transfer function *G*(s) of the servo electric cylinder is derived as:

$$G(s)=\frac{L_x(s)}{U(s)}=\frac{K_t p_h}{2n\pi s(LJS^2+(RJ+BL)S+BR+K_e K_t)} \quad (12)$$

The dynamic model of the servo electric cylinder, along with the mathematical model of the transmission system, establishes a foundation for subsequent simulations and the decoupling control of leveling and profiling motions.

Control Strategy Design

While Active Disturbance Rejection Control (ADRC) exhibits strong disturbance rejection for handling model uncertainties, its Extended State Observer (ESO) may lag under rapidly changing disturbances, degrading transient performance. In contrast, Super-Twisting Sliding Mode Control (ST-SMC) provides finite-time convergence, strong robustness, and reduced chattering. However, ST-SMC is sensitive to parameter variations and cannot independently address motion coupling or dynamic parameter changes.

To address these issues in the transplanter's synergistic leveling and profiling system, the ESO is integrated into the ST-SMC framework. The ESO estimates and compensates for total disturbances in real time, thereby reducing sliding surface uncertainties. Concurrently, the Super-Twisting algorithm ensures finite-time error convergence. The control law synthesizes the error feedback of ADRC with the reaching law of ST-SMC. This integrated controller actively cancels disturbances, maintains robust stability, and eliminates chattering.

The integrated Super-Twisting Sliding Mode Active Disturbance Rejection Controller is shown in Fig. 9. The disturbance estimation output z3 from the Extended State Observer is fed into the Super-Twisting Sliding Mode Controller.

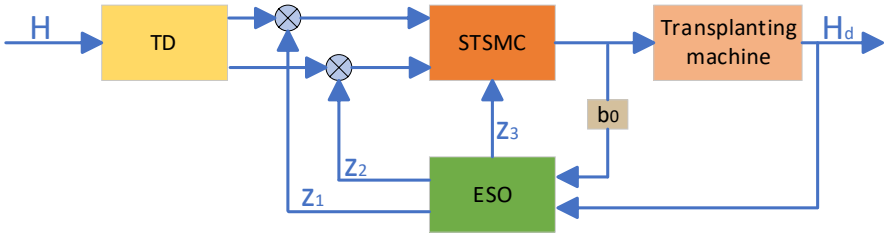

Fig. 9 - Super-twisting sliding mode active disturbance rejection controller

Sliding Mode Control Design

The Super-Twisting Sliding Mode Control primarily consists of two parts: the design of the sliding surface and the design of the sliding mode control law. Defining the height error as e_{1H} and its derivative as e_{2H}, the sliding surface s is designed using the height channel as an example:

$$s_H = e_{2H} + \lambda_H \bullet e_{1H} \quad (13)$$

where λ_H is the sliding surface coefficient, and its value is greater than zero.

Super-Twisting Sliding Mode Control Law Design:

$$\begin{cases} \dot{v} = -k_2 sign(s) \\ u_{sH} = -k_1\sqrt{|s|}sign(s)+v \\ u_{cH} = -\dfrac{z_{H3}}{b_0} \\ u_H = u_{sH}+u_{cH} \end{cases} \quad (14)$$

where k_1 and k_2 are gain parameters.

Extended State Observer Design

The synergistic control system for transplanter leveling and profiling is subjected to external disturbances originating from both the transplanter itself and the system during operation. Furthermore, synergistic control introduces coupling effects between the leveling and profiling functions. The Extended State Observer (ESO) possesses the capability to estimate the total disturbance and achieve dynamic compensation, thereby eliminating these coupling effects.

Taking the profiling channel as an example, the established Extended State Observer is as follows:

$$\begin{cases} e_H = z_{H1} - H \\ \dot{z}_{H1} = z_{H2} - \beta_{H1} fal(e_H, \alpha_{H1}, \delta_H) \\ \dot{z}_{H2} = z_{H3} - \beta_{H2} fal(e_H, \alpha_{H2}, \delta_H) + b_{H0} u_{H3} \\ \dot{z}_{H3} = -\beta_{H3} fal(e_H, \alpha_{H3}, \delta_H) \end{cases} \quad (15)$$

$$fal(x, \alpha_H, \delta_H) = \begin{cases} \dfrac{x}{\delta_H^{(1-\alpha_H)}}, |x| \le \delta_H \\ sign(x)|x|^{\alpha_H}, |x| > \delta_H \end{cases} \quad (16)$$

In the equations, H represents the angle of the controlled plant, u_{H3} is the input to the controlled plant, $\beta_{H1}, \beta_{H2}, \beta_{H3}$ are the observer feedback gains, ω_0 is the observer bandwidth, b_0 is the gain parameter, and δ is the linear interval width of the *fal* function.

Integrated STSMC-ESO Control Law

As derived from the transplanter system model, the synergistic control system for lateral leveling and longitudinal profiling consists of a leveling channel and a profiling channel. The block diagram of this synergistic control system is illustrated in Fig. 10.

Equations (8) and (9) indicate the presence of mutual coupling between the leveling angle and the profiling height within the transplanter model, making its design challenging. However, the Extended State Observer (ESO) possesses inherent decoupling capabilities, allowing for a simplification of the system model.

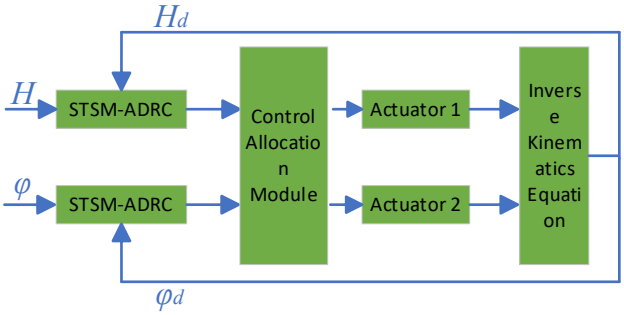

Fig. 10 - Block diagram of the synergistic control system for the transplanter

Stability Analysis

A stability analysis is conducted for the Super-Twisting Sliding Mode Control. Based on the design of the Extended State Observer (ESO), where z_{H1} estimates x_1, z_{H2} estimates x_2, and z_{H3} estimates x_3, the dynamic model of the servo motor is rewritten in state-space form as:

$$\begin{cases} \dot{z}_{H1} = z_{H2} \\ \dot{z}_{H2} = a_0 u - a_1 z_{H2} - W(t) \end{cases} \quad (17)$$

where z_{H1}, z_{H2}, and z_{H3} are the outputs of the Extended State Observer. Assuming the outputs z_{H1}, z_{H2}, and z_{H3} of the Extended State Observer are bounded, all disturbances in the system except those related to the motor are defined as the total disturbance $W(t)$. In equation (17), $a_0 = K_t/J$, $a_1 = B/J$。

Taking the profiling channel as an example, the height error is defined as:

$$\begin{cases} e_{1H} = z_{H1} - H_a \\ e_{2H} = \dot{e}_{1H} = z_{H2} - \dot{H}_a \end{cases} \quad (18)$$

Differentiating the sliding surface s_H yields:

$$\dot{s}_H = \dot{e}_{2H} + \lambda_H \bullet \dot{e}_{1H} \quad (19)$$

Combining equations (17) - (19) yields:

$$\dot{s}_H = -a_0 k_1 \sqrt{|s|} sign(s) + a_0 v - \frac{a_0 z_{H3}}{b_0} - a_1 z_{H2} - W(t) - \ddot{H}_a + \lambda_H \dot{z}_{H2} - \lambda_H \dot{H}_a \quad (20)$$

In the equation, the target value H_a is a constant, and all disturbances in the system can be estimated by $W(t)$, resulting in:

$$\dot{s}_H = -a_0 k_1 \sqrt{|s|} sign(s) + a_0 v + W(t) \quad (21)$$

The Lyapunov function is defined as:

$$V = \alpha |s| + \frac{1}{2} v^2 \quad (22)$$

where α>0 is a parameter to be determined. This function is positive definite and radially unbounded.

Its derivative is:

$$\dot{V} = \alpha \bullet \dot{s} \bullet sign(s) + v\dot{v} \quad (23)$$

Combining equations (22) and (23) yields:

$$\dot{V} = -\alpha a_0 k_1 \sqrt{|s|} + sign(s) \bullet (\alpha a_0 v - k_2 v + w) \quad (24)$$

According to the Lyapunov stability theory, in order to ensure that Eq. (24) is less than 0, the coefficient k_1 of the negative dominant term is large enough. Since the differential result of v is an item in Eq.(14), the above equation can be established by selecting the appropriate parameters λ_H, k_1, k_2. According to the proof results, the differential of the constructed Lyapunov function is less than zero, that is, it is semi-negative definite. The system is asymptotically stable, and its synovial surface s eventually converges to zero, so as to realize the tracking of the target trajectory.

Simulation Experiments

Simulation Platform Construction

To validate the performance of the Super-Twisting Sliding Mode Active Disturbance Rejection Controller (STSMC-ADRC) within the transplanter's synergistic leveling and profiling control system, a co-simulation approach utilizing Adams and MATLAB/Simulink is adopted in this study. A simplified model of the complete transplanter and a ground model are created in SolidWorks and subsequently imported into Adams. Within Adams, constraints are applied to define the kinematic relationships between the swing mechanisms, servo electric cylinders, rear axle, and wheels, thereby simulating realistic leveling motions. MATLAB/Simulink is employed to build the synergistic leveling and profiling control system. The model is imported via the Adams/Controls interface to establish the co-simulation platform. Based on the STSMC-ADRC and the servo electric cylinder mathematical model developed in the previous section, C code is written and integrated into MATLAB/Simulink, where the controller and actuator models are implemented. The relevant parameters configured for the servo electric cylinder are listed in Table 1.

Table 1

Simulation Parameters of Servo Electric Cylinder

Description	Unit	Values
Torque constant K_t	N.m/A	0.13
Lead of the screw p_h	mm	10
Gear reduction ratio n	1	7
Armature inductance L	mH	0.17
Rotor moment of inertia J	kg·m^2	2.2×10^{-4}
Armature resistance R	Ω	0.05
Viscous friction coefficient B	N·m·s/rad	4.33×10^{-6}
Back electromotive force constant K_e	V/rad	8×10^{-3}

The structure of the co-simulation system is illustrated in Fig. 11.

A lateral inclination sensor is installed on the transplanter body, and a displacement sensor is mounted at the rear. The real-time output data of the vehicle's lateral inclination and displacement are fed back as inputs to the Super-Twisting Sliding Mode Active Disturbance Rejection Controller (STSMC-ADRC). The STSMC-ADRC processes the inclination and displacement signals, performs synergistic computation on the output angle and displacement signals, and converts them into input signals for the two motors. These signals are then input to the transfer functions of the left and right servo electric cylinders, respectively, to obtain the displacement signals for the cylinders. These displacement signals are subsequently fed into the Adams_sub module. The movement of the two electric cylinders drives the swing mechanisms, causing the vehicle's roll angle error to approach 0° and the displacement target value to reach 50 mm, thereby achieving the co-simulation of the transplanter's leveling process.

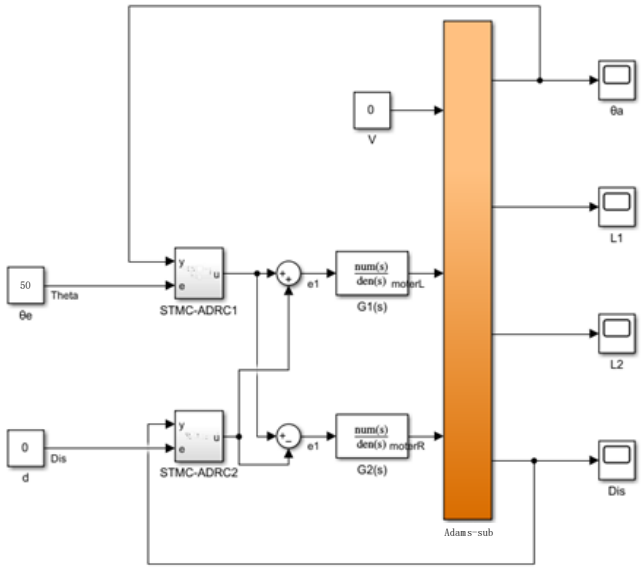

Fig. 11 - Joint simulation model of leveling and contouring collaborative control system for transplanting machine

Simulation Testing under Typical Working Conditions

Synergistic Leveling and Profiling

The established co-simulation model was executed in MATLAB/Simulink to evaluate the performance of the three algorithms—PID, ADRC, and STSMC-ADRC—at speeds of 0.2 m/s, 0.3 m/s, and 0.4 m/s. Fig.12 shows the angle variation curves during synergistic control under these different speeds. The shaded area under each curve represents the integral area between the curve and the target value.

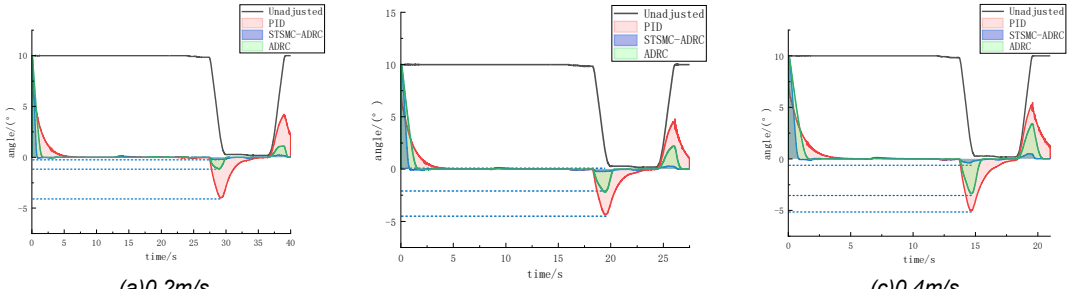

(a)0.2m/s *(b)0.3m/s* *(c)0.4m/s*

Fig. 12 - Collaborative control of different speed and angle outputs

Table 2 is the area enclosed by the angle curve and the target value of different algorithms at different speeds.

Table 2

Area Enclosed by the Angle Curve and the Target Value at Different Speeds

Control Algorithm	0.2 m/s	0.3 m/s	0.4 m/s
PID	29.84	23.16	22.85
STSMC-ADRC	5.48	5.31	5.42
ADRC	10.85	12.16	13.53

Table 2 is the lowest point of the angle curve at different speeds. Under the condition of 0.2 m/s speed and 40 s simulation time, the area enclosed by the PID angle control and the target value of 0 ° is 29.84, and the lowest point of the curve is - 3.99°. The area of the curve formed by the angle control of STSMC-ADRC and the target value of 0 ° is 5.48, and the lowest point of the curve is − 0.29°. The curve area of ADRC angle control and target value 0 ° is 10.85, and the lowest point of the curve is - 1.12 °. Under the condition of speed of 0.3 m/s and simulation time of 27.5 s, the curve area of PID angle control and target value of 0 ° is 23.16, and the lowest point of the curve is - 4.33°. The area of the curve formed by the angle control of STSMC-ADRC and the target value of 0° is 5.31, and the lowest point of the curve is - 0.31°. The curve area of ADRC angle control and target value 0° is 12.16, and the lowest point of the curve is - 2.21°. Under the condition of speed of 0.4 m/s and simulation time of 21 s, the area of the curve formed by PID angle control and target value of

0° is 22.85, and the lowest point of the curve is - 5.01°. The area of the curve formed by the angle control of STSMC-ADRC and the target value of 0° is 5.42, and the lowest point of the curve is - 0.47°. The curve area of ADRC angle control and target value 0° is 13.527, and the lowest point of the curve is - 3.37°.

At a speed of 0.2 m/s, the integrated angle error area for PID control was 29.84, while those for STSMC-ADRC and ADRC were 5.48 and 10.85, respectively. Compared to PID, STSMC-ADRC reduced the error area by 81.6%, and ADRC reduced it by 63.6%. The lowest point reached by PID was -3.99°, whereas STSMC-ADRC and ADRC achieved -0.29° and -1.12°, respectively. This indicates that the overshoot of STSMC-ADRC was reduced by approximately 92.7% compared to PID, while ADRC achieved a 71.9% reduction.

At a speed of 0.3 m/s, the integrated error area for PID control was 23.16, while those for STSMC-ADRC and ADRC were 5.31 and 12.16, respectively. STSMC-ADRC reduced the error area by 77.1% compared to PID, while ADRC achieved a 47.5% reduction. Regarding the lowest point, PID reached -4.33°, whereas STSMC-ADRC and ADRC reached -0.31° and -2.21°, respectively. This represents a 92.8% reduction in the lowest point deviation for STSMC-ADRC and a 48.9% reduction for ADRC, both compared to PID.

At a speed of 0.4 m/s, the integrated error area for PID control was 22.85, while the values for STSMC-ADRC and ADRC were 5.42 and 13.53, respectively. This represents a 76.3% reduction in the error area for STSMC-ADRC compared to PID, while ADRC achieved a 40.8% reduction. Regarding the lowest point, PID reached -5.01°, whereas STSMC-ADRC and ADRC reached -0.47° and -3.37°, respectively. This corresponds to a 90.6% reduction in the lowest point deviation for STSMC-ADRC and a 32.7% reduction for ADRC, both compared to PID.

In summary, the STSMC-ADRC controller significantly outperforms both ADRC and PID across all three tested speeds, maintaining a stable integrated angle error area of approximately 5. In contrast, ADRC demonstrates intermediate performance, exhibiting a deteriorating trend as speed increases. PID control performs the poorest, with its errors increasing significantly at higher speeds.

Table 3

Lowest Points of Angle Curves at Different Speeds

Control Algorithm	0.2 m/s	0.3 m/s	0.4 m/s
PID	-3.99	-4.33	-5.01
STSMC-ADRC	-0.29	-0.31	-0.47
ADRC	-1.12	-2.21	-3.37

Fig. 13 illustrates the displacement output of the cooperative control under different operating speeds. The shaded areas enclosed by each curve and the target value represent the deviation area between the actual response and the desired trajectory.

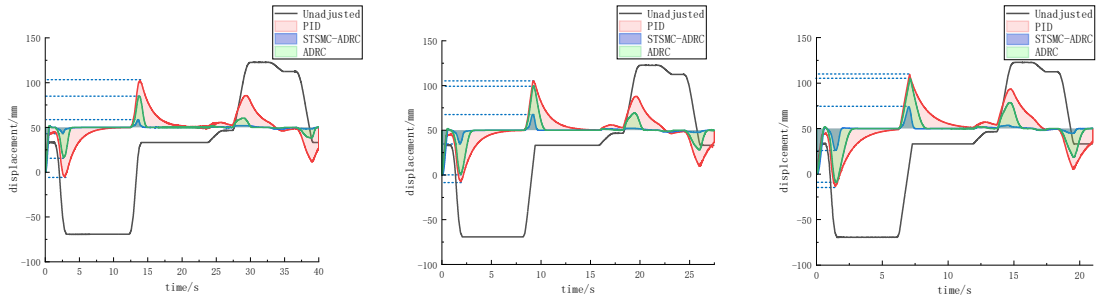

(a)0.2m/s *(b)0.3m/s* *(c)0.4m/s*

Fig. 13 - Collaborative Control of Displacement Output at Different Speeds

Under the condition that the speed is 0.2 m/s and the simulation time is 40 s, the area of the curve formed by the PID displacement control and the target value of 50 mm is 296.07, the lowest point is − 4.59 mm and the highest point is 102.52 mm. The curve area of the displacement control of the STSMC-ADRC and the target value of 50 mm is 33.35, the lowest point is 44.65 mm, and the highest point is 59.54 mm; the curve area of ADRC displacement control and target value 50 mm is 91.72, the lowest point is 17.17 mm, and the highest point is 84.85 mm.

Under the condition of speed of 0.3 m/s and simulation time of 27.5 s, the curve area of PID displacement control and target value of 50 mm is 372.15, the lowest point is - 7.32 mm, and the highest point is 104.83 mm. The curve area of the displacement control of the STSMC-ADRC and the target value of 50 mm is 50.83, the lowest point is 35.75 mm, and the highest point is 67.95 mm. The curve area of ADRC displacement control and target value 50 mm is 156.20, the lowest point is 1.75 mm, the highest point is 98.13 mm.

Under the condition of speed of 0.4 m/s and simulation time of 21s, the curve area of PID displacement control and target value of 50 mm is 359.90, the lowest point is-13.21 mm, and the highest point is 109.08 mm. The curve area of the displacement control of the STSMC-ADRC and the target value of 50 mm is 56.44, the lowest point is 25.95 mm, and the highest point is 74.69 mm; the curve area of ADRC displacement control and target value 50 mm is 178.03, the lowest point is - 9.09 mm, and the highest point is 103.44 mm.

Table 4

Area Between the Displacement Curve and the Target Value at Different Speeds

Control Algorithm	0.2 m/s	0.3 m/s	0.4 m/s
PID	296.07	372.15	359.90
STSMC-ADRC	33.35	50.83	56.44
ADRC	91.72	156.20	178.03

In terms of displacement control, the differences between the three methods are even more pronounced. As shown in Tables 4, 5, and 6, at a speed of 0.2 m/s, the integrated error area for PID control is as high as 296.07, while the values for STSMC-ADRC and ADRC are 33.35 and 91.72, respectively. This represents an 88.7% reduction in the error area for STSMC-ADRC and a 69.0% reduction for ADRC, both compared to PID. Regarding the displacement fluctuation range, PID exhibits a minimum point of -4.59 mm and a maximum point of 102.52 mm, resulting in a range of 107.1 mm. In contrast, the range for STSMC-ADRC is only 14.9 mm, representing an 86.1% reduction compared to PID, while ADRC shows a range of 67.7 mm, a 36.8% reduction compared to PID.

At speeds of 0.3 m/s and 0.4 m/s, the integrated error areas for STSMC-ADRC are 50.83 and 56.44, respectively, representing reductions of 86.4% and 84.3% compared to PID control. Concurrently, its displacement fluctuation ranges are reduced by 71.3% and 60.2%, respectively, compared to PID. In contrast, the integrated error area for ADRC is significantly higher than that of STSMC-ADRC and progressively deteriorates with increasing speed, reaching approximately 0.5 times that of PID at 0.4 m/s.

Table 5

Minimum Points of Displacement Curves at Different Speeds

Control Algorithm	0.2 m/s	0.3 m/s	0.4 m/s
PID	-4.59	-7.32	-13.21
STSMC-ADRC	44.65	35.75	25.95
ADRC	17.17	1.75	-9.09

Table 6

Maximum Points of Displacement Curves at Different Speeds

Control Algorithm	0.2 m/s	0.3 m/s	0.4 m/s
PID	102.52	104.83	109.08
STSMC-ADRC	59.54	67.95	74.69
ADRC	84.85	98.13	103.44

In summary, the STSMC-ADRC algorithm, owing to its inherent robustness and finite-time convergence properties, enables rapid and smooth error elimination while exhibiting strong insensitivity to system parameter variations and external disturbances. Its average integral absolute error for displacement control is merely 12.5% of that of PID and 33.8% of that of ADRC, establishing it as the optimal solution for achieving high-precision profiling control. Although ADRC compensates for certain system uncertainties through its disturbance observer and outperforms PID, its observer performance and controller parameters require further optimization under varying operational conditions to enhance its adaptive capability and stability. The conventional PID controller demonstrates unsatisfactory performance in this application due to its inherent difficulty in handling the system's nonlinearities and strong coupling characteristics.

RESULTS AND DISCUSSION

Field Dynamic Test Results

Field experiments were conducted at the Zhongnong Futong Horticulture Co., Ltd. in Tongzhou District, Beijing. Fig.14 shows the field test scenario of the transplanter. A ridged field with undulating terrain was designed, as shown in Fig.14(a), where the ridge height variation was 100 mm, to evaluate the profiling performance of the transplanter. A terrain for testing body leveling was designed, as shown in Fig.14(b), featuring a height difference of approximately 240 mm between the left and right furrows, with a rear wheel track of 1400 mm.

(a) Ridge profiling *(b) Vehicle body leveling*

Fig. 14 - Field Experiment Scene

Fig.15 shows the angle adjustment of the transplanter after activating synergistic control at a speed of 0.3 m/s, with the shaded area representing the range of ±1.5°. Under the STSMC-ADRC control algorithm, the integrated absolute error (IAE) between the curve and the target value of 0° is 10.94, with a minimum value of -1.34° and a maximum value of 1.09°. Under the ADRC control algorithm, the IAE is 24.80, with a minimum value of -3.03° and a maximum value of 3.39°. Under the PID control algorithm, the IAE is 35.62, with a minimum value of -4.62° and a maximum value of 4.56°.

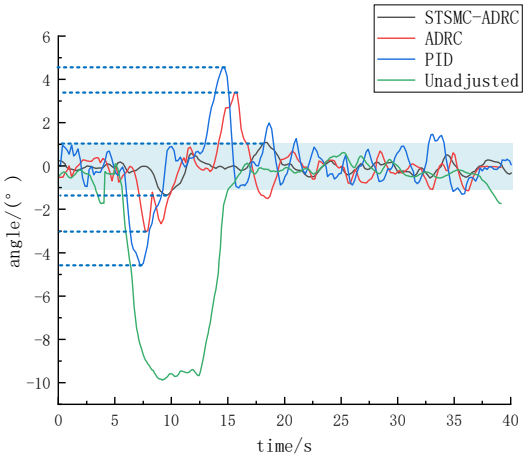

Fig. 15 - Angle adjustment at a speed of 0.3 m/s

Fig.16 shows the displacement adjustment of the transplanter after activating synergistic control at a speed of 0.3 m/s, with the shaded area representing the range of 50 ± 10 mm. Under the STSMC-ADRC control algorithm, the integrated absolute error (IAE) between the curve and the target value of 50 mm was 134.55, with a minimum value of 37.80 mm and a maximum value of 83.38 mm. Under the ADRC control algorithm, the IAE was 213.39, with a minimum value of 26.76 mm and a maximum value of 125.32 mm. Under the PID control algorithm, the IAE was 385.36, with a minimum value of 9.65 mm and a maximum value of 155.15 mm.

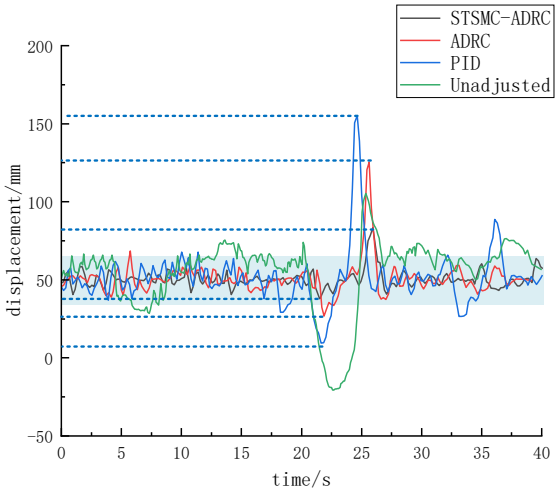

Fig. 16 - Displacement adjustment at a speed of 0.3 m/s

As shown in Table 7, the integrated absolute error (IAE) for the angle under STSMC-ADRC control is 10.94, while the values for ADRC and PID are 24.80 and 35.62, respectively. Compared to PID, STSMC-ADRC reduces the error area by 69.3%, and it achieves a 55.9% reduction compared to ADRC. This demonstrates that STSMC-ADRC can significantly enhance the steady-state accuracy of the system in disturbance-prone environments. Regarding dynamic response, the angle fluctuation range of STSMC-ADRC is only from -1.34° to 1.09°, with the overall deviation not exceeding ±1.5°. In contrast, ADRC and PID exhibit ranges of up to ±3.2° and ±4.6°, respectively. The dynamic deviation of STSMC-ADRC is reduced by approximately 67% compared to PID. This indicates that the proposed algorithm can rapidly suppress overshoot during the leveling process and significantly reduce system oscillation.

In profiling control, the integrated absolute error (IAE) for displacement under STSMC-ADRC is 134.55, while the values for ADRC and PID are 213.39 and 385.36, respectively. This represents a reduction of 65.1% compared to PID and a 37.0% reduction compared to ADRC. The minimum and maximum values for STSMC-ADRC are 37.80 mm and 83.38 mm, respectively, resulting in a fluctuation range of approximately 45.6 mm. In contrast, the fluctuation ranges for ADRC and PID expand to 98.6 mm and 145.5 mm, respectively. These results demonstrate that the disturbance suppression capability of STSMC-ADRC for displacement is approximately 3.2 times more effective than that of PID control.

Table 7

Performance Comparison of Control Algorithms at 0.3 m/s

Control Algorithm	Angular Error Area	Angular Range (°)	Displacement Error Area	Displacement Range (mm)
STSMC-ADRC	10.94	-1.34~1.09	134.55	37.80~83.38
ADRC	24.80	-3.03~3.39	213.39	26.76~125.32
PID	35.62	-4.62~4.56	385.36	9.65~155.12

Field Planting Test Results

Fig.17 shows the field planting performance from the experiment. The planting conditions were identical to the field dynamic test conditions, with a traveling speed of 0.3 m/s. The shaded area in the Figure represents the region of qualified planting performance.

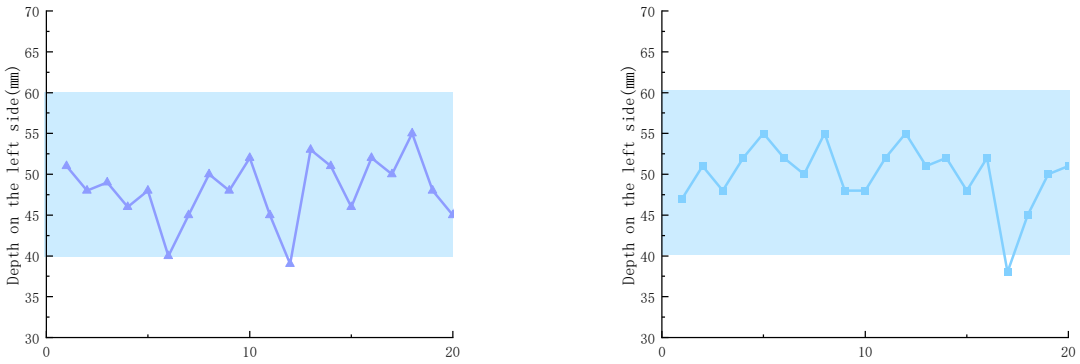

(a) Planting depth on the left side *(b) Planting depth on the right side*

Fig. 17 - Planting Depth on Both Sides at a Speed of 0.3 m/s

The overall average planting depth was 49.1 mm, deviating from the target value of 50.0 mm by only -0.9 mm, resulting in a relative error of merely 1.8%. The average depth on the left side was 48.7 mm, and on the right side was 49.5 mm, with a mere 0.8 mm difference between the two sides. The standard deviation for the overall dataset was 4.0 mm. Despite the presence of occasional strong disturbances causing the planting depth to deviate from the target zone, the STSMC-ADRC algorithm was able to rapidly restore the depth to near the target value. This demonstrates the strong disturbance estimation and robust control capabilities of the Super-Twisting Sliding Mode Active Disturbance Rejection Controller.

CONCLUSIONS

(1) When the transplanting mechanism works dynamically, the system parameters vary with the impact caused by uneven ground, different planting resistance of duckbill, and different operating speeds. There is a strong nonlinearity, and it is difficult to establish an accurate mathematical model. And the traditional motion control PID control has the problem of weak anti-disturbance ability, and the modern active disturbance

rejection control may lag in the estimation and compensation of severe and high frequency disturbances. In this paper, the super-twisting synovial auto-disturbance rejection control algorithm is proposed and applied to the leveling and profiling cooperative control system of the transplanter. The results show that after starting the cooperative control simulation, in terms of angle adjustment, when the speed is 0.2 m/s, compared with PID, the error area of STSMC is reduced by 81.6 %, and ADRC is reduced by 63.6 %. At 0.3 m/s, STSMC is reduced by 77.1 % compared with PID, and ADRC is reduced by 47.5 %. At 0.4 m/s, STSMC is 76.3 % lower than PID and ADRC is 40.8 % lower. STSMC is significantly better than ADRC and PID at three speeds, and the performance of ADRC is between the two, showing a deterioration trend with the increase of speed. PID has the worst performance, and the error increases significantly with the increase of speed.

(2) To address the issue of inconsistent single-row and multi-row planting depths in multi-row transplanters operating on slopes or ridges with uneven height differences—a problem where traditional control systems lack rule-based decision-making capabilities and struggle to achieve synergistic control—this study employs the disturbance estimation of the Super-Twisting Sliding Mode Active Disturbance Rejection Control (STSMC-ADRC) to achieve decoupled control of the transplanter's leveling and profiling. Simultaneously, building upon existing research and industry standards, planting depth is adopted as the evaluation metric.

REFERENCES

[1] Cai Z., (2023). Design and Experiment of Attitude Adjustment System for High Ground Gap Pla nt Protection Machine (高地隙植保机车身姿态调节系统设计与试验). *Anhui Agricultural University*, Anhui / China.

[2] Chao K., Shou X., Cheng D., Fan L., Jun L., (2023). Design and test of automatic leveling system for transplanter in hilly and mountainous areas (丘陵山地移栽机自动调平系统设计与试验). *Journal of Chinese Agricultural Mechanization*, Vol. 44, pp. 17, Nanjing/China. https://doi.org/10.13733/j.jcam.issn.2095-5553.2023.08.003

[3] Cui Z., Guan C., Yang Y., Gao Q., Chen Y., Xiao T., (2020). Research status of vegetable mechanical transplanting technology and equipment (蔬菜机械化移栽技术与装备研究现状). *Journal of Chinese Agricultural Mechanization*, Vol. 41, pp.85-92. Jiangsu/China https://doi.org/10.13733/j.jcam.issn.2095-5553.2020.03.015

[4] Cui W., (2015). *Research on Dry Land Automatic Transplanter for Plug Seedling (旱地钵体苗自动移栽机理论与试验研究).* China Agricultural University, Beijing / China.

[5] Chen B., Yin D., Lu C., Zhang Z., Zhang H., Ji H., (2015). Overview and Development Considerations of Transplanting Agricultural Machinery (移栽农机具概况与发展思考). *Agricultural Mechanization Research*, Vol. 3, pp. 258-263, Heilongjiang/China. https://doi.org/1003－188X（2015）03－0258－06

[6] Cai G., Li H., Li H., Wang Q., He J., Ni J., (2011). Design of test-bed for automatic depth of furrow opening control system based on ATmega128 single chip microcomputer (基于 ATmega128 单片机的开沟深度自控系统试验台的设计). *Transactions of the Chinese Society of Agricultural Engineering*, Vol. 27, pp. 11-16, Beijing/China. https://doi.org/10.3969/j.issn.1002-6819.2011.10.002

[7] Denis D., Thuilot B., Lenain R., (2016). Online adaptive observer for rollover avoidance of reconfigurable agricultural vehicles. *Computers and electronics in agriculture*, Vol. 126, pp. 32-43, Netherlands. https://doi.org/10.1016/j.compag.2016.04.030

[8] Hou P., (2023). Research on Body Leveling System of Small Self-propelled Corn Harvester (小型自走式玉米收获机车身调平系统研究). *Jilin University*, Jilin/China.

[9] Han Z., Yan H., Chen K., He Y., (2018). Application status and prospect of planting depth profiling technology for transplanting machinery (移栽机械栽植深度仿形技术应用现状及展望). *Agricultural Engineering*, Vol. 8, pp. 1-7, Beijing/China. https://doi.org/2095-1795(2018)04-0001-07

[10] Han B., Yang Y., Wang H., Fan W., (2018). Design of PID automatic control system for depth into earth of intra-row weeding components and its bench experiment (苗间除草部件入土深度 PID 自动控制系统设计与台架试验). *Transactions of the Chinese Society of Agricultural Engineering,* Vol. 34, pp. 68-77, Beijing/China. https://doi.org/10.11975/j.issn.1002-6819.2018.11.009

[11] He Z., Zheng Z., Liu J., Ji J. (2014). Current Status and Existing Problems of Film-Based Transplanters (膜上移栽机的发展现状及存在的问题). *Agricultural Mechanization Research*, Vol. 9, pp. 252-255, Heilongjiang/China. https://doi.org/1003-188X(2014)09-0252-04

[12] Ji D., Tian S., Wu H., Zhao B., Gong Y., Ma J., Liu W., (2023). Design and experimental verification of an automatic transplant device for a self-propelled flower transplanter. *Journal of the Brazilian Society of Mechanical Sciences and Engineering*, Vol. 45, pp. 420, Brazil. https://doi.org/10.1007/s40430-023-04256-0

[13] Li M., Zhao J., Zhu Z., Xie B., Chi R., Mao E., (2013). Fuzzy-PID self-adaptive control method in electro-hydraulic hitch system (拖拉机电液悬挂系统模糊 PID 自适应控制方法). *Transactions of the Chinese Society for Agricultural Machinery*, Vol. 44, pp. 295-300, Beijing/China. https://doi.org/10.6041/i.issn.1000-298.2013.S2.055

[14] Lee S. S., Oh K. S., Hwang H., Choi D. Y., (2000). Automatic leveling control system for combine. *IFAC Proceedings Volumes*, Vol. 33, pp. 255-258, Austria. https://doi.org/10.1016/S1474-6670(17)36786-1

[15] Ma Y., Li R., Xu J. (2019). Research on fuzzy PID automatic control strategy for tractor tillage depth (拖拉机耕深模糊 PID 自动控制策略研究). *Agricultural Mechanization Research*, Vol. 41, pp. 241-247, Heilongjiang/China. https://doi.org/1003-188X(2019)01-0241-07

[16] McCool W. D. K., (2010). William F. Schillinger Dep. of Crop and Soil Sciences, Washington State University, Dryland Research Station, Lind, WA Robert I. Papendick retired, formerly USDA-ARS, Land Management and Water Conservation Research. *Soil and Water Conservation Advances in the United States*, Vol. 60, pp. 47, United States.

[17] Ping L., Feng P., Hai L., Zhuang W., Wen W., Jun Z., (2017). Design and Experiment of Adaptive Leveling Chassis for Hilly Area (丘陵山区农用自适应调平底盘设计与试验). *Transactions of the Chinese Society of Agricultural Machinery*, Vol. 48, Beijing/China. https://doi.org/10.6041/j.issn.1000-1298.2017.12.005

[18] Somefun O. A., Akingbade K., Dahunsi F., (2021). The dilemma of PID tuning. *Annual Reviews in Control*, Vol. 52, pp. 65-74, Netherlands. https://doi.org/10.1016/j.arcontrol.2021.05.002

[19] Sun Y., Xu L., Jing B., Chai X., Li Y., (2020). Development of a four-point adjustable lifting crawler chassis and experiments in a combine harvester. *Computers and Electronics in Agriculture*, Vol. 173, Netherlands. https://doi.org/10.1016/j.compag.2020.105416

[20] S Schillinger W. F., Papendick R. I., McCool D. K., (2010). Soil and water challenges for Pacific Northwest agriculture. *Soil and water conservation advances in the United States*, Vol. 60, pp. 47-79, United States. https://doi.org/10.2136/sssaspecpub60.c2

[21] Saeys W., Engelen K., Ramon H., Anthonis J., (2007). An automatic depth control system for shallow manure injection, Part 1: Modelling of the depth control system. *Biosystems Engineering*, Vol. 98, pp. 146-154, United Kingdom. https://doi.org/10.1016/j.biosystemseng.2007.06.002

[22] Tang K. S., Man K. F., Chen G., Kwong S., (2001). An optimal fuzzy PID controller. *IEEE transactions on industrial electronics*, Vol. 48, pp. 757-765, United States. https://doi.org/10.1109/41.937407

[23] Wu W., Sun S., Xiao M., (2013). Current Status and Development Trends of Transplanters in China (我国移栽机械的现状与发展趋势). *Agricultural Technology and Equipment*, Vol. 12, pp. 7-8,10, Shanxi/China. https://doi.org/10.3969/j.issn.1673-887X.2013.06.003

[24] Xiao M., Xiao S., Sun S., Chen B., Chen S., (2019). Research Status and Development Trends of Oilseed Rape Seedling Transplanting Mechanisms (油菜钵体苗移栽机构研究现状与发展趋势). *Agricultural Mechanization Research*, Vol. 41, pp. 1-6, Heilongjiang/China. https://doi.org/1003-188X(2019)12-0001-06

[25] Ye F., (2023). Design and simulation of track chassis and active levelling device in hilly region (丘陵山地履带底盘与主动调平装置的设计与仿真). *Jiangxi University of Science and Technology*, Jiangxi/China.

[26] Yang Y., Cheng S., Qi J., Qi J., Zhang G., Ma Q., (2022). Design and Test of Automatic Leveling System for Agricultural Machinery Seat Based on Ergonomics (基于人机工效学的农机座椅自动调平系统设计与试验). *Transactions of the Chinese Society for Agricultural Machinery*, Vol. 53, pp. 434-442, Beijing/China. https://doi.org/10.6041/j.issn.1000-1298.2022.06.046

[27] Yang Y. (2007). Research of header height automatic controlling system based on ultrasonic sensor (基于超声波传感器的割台高度自动控制系统研究). *Northwest A&F University*, Shanxi/China.

[28] Zhou M., Wang G., Zhang Y., Yang J., Wei Z., Sun H., Yin J., (2024). Design and test of walk-type rice potted seedling transplanting machine. *Advances in Mechanical Engineering*, Vol.16, United States. https://doi.org/10.1177/16878132241237710

[29] Zhang F., Lyu X., Yang H., Du L., Liu Z., Tang P., Lyu X., (2023). Design of leveling system for mountain tractor based on fuzzy PID (基于模糊 PID 的山地拖拉机调平控制系统的设计). *Journal of Hunan Agricultural University (Natural Sciences)*, Vol. 49, pp. 121-126, Hunan/China. https://doi.org/10.13331/j.cnki.jhau.2023.01.017

[30] Zhang Q., Liao Q., Xiao W., Liu X., Wei G., Liu L., (2018). Research process of tillage technology and equipment for rapeseed growing (油菜种植耕整地技术装备研究与发展). *Chinese journal of oil crop sciences*, Vol. 40, pp. 702-711, Hubei/China. https://doi.org/10.7505/j.issn.1007-9084.2018.05.013